Orientational Imaging of Single Molecules by Annular Illumination

B. Sick and B. Hecht*
Physical Chemistry Laboratory, Swiss Federal Institute of Technology, ETH-Z, CH-8092 Zürich, Switzerland

L. Novotny
The Institute of Optics, University of Rochester, Rochester, New York 14627
(Received 25 April 2000)

The absorption dipole orientation of single fluorescent molecules is determined by mapping the spatial distribution of the squared electric field components in a high-numerical-aperture laser focus. Annular illumination geometry and the vicinity of a plane dielectric/air interface strongly enhance the longitudinal field component and the transverse fields perpendicular to the polarization direction. As a result, all three excitation field components in the focus are of comparable magnitude. The scheme holds promise to monitor rotational diffusion of single molecules in complex environments.

PACS numbers: 33.70.Ca, 07.79.–v, 87.64.Tt

The ability to detect single molecules at room temperature [1,2] at surfaces [3–5] has opened a wide field of applications including biology [6,7], biochemistry [8], material sciences [9], and quantum optics [10]. Single molecules have been used as markers and local probes for molecular processes in their immediate environment [7,8]. An important parameter in single molecule experiments is the orientation of the absorption dipole moment (for a review see [11]). Reorientation of the dipole moment can be caused by subtle changes in the chromophores environment [7] or reveal degrees of freedom in the spatial organization of moieties within macromolecules by observation of hindered rotational diffusion [12]. Furthermore, various relevant observables in single-molecule experiments such as lifetime [4] and fluorescence quantum yield [13] are influenced by the dipole orientation. Knowledge of relative orientation is also a prerequisite for precise distance measurements using single-pair fluorescence resonant energy transfer [14].

As a matter of fact, standard polarization microscopy, apart from special cases [15], allows one to determine only the components of the absorption [7] or the emission dipole moments [12,16] in the plane of the substrate. Emission patterns of single molecules obtained in defocused [17] or aberrated wide-field microscopy through thick water layers [18] and scanning near-field optical microscopy [3,5], respectively, have been interpreted with respect to the three-dimensional dipole orientation. In the first two cases, defocusing or aberrated imaging reveals additional structure in single-molecule emission patterns that depends on the orientation of the emitting dipole. However, the spatial resolution is diminished. In the second case, the absorption dipole moment of a molecule maps the spatial distribution of the squared exciting electric field component along its direction. The obtained patterns can be used to conclude about the dipole orientation if the electric field distribution can be reliably predicted. This is, however, a time consuming task, and in many cases difficult because of lacking nanometer scale structural data of the optical probe.

In the present Letter we report on orientational imaging of single dye molecules embedded in a thin polymer film on a cover glass using scanning confocal optical microscopy. Single molecules are excited by a focused annular laser beam at normal incidence to the interface. This yields a considerably enhanced longitudinal electric field component. In addition, due to the proximity of the interface, the in-plane field component perpendicular to the linear excitation polarization is increased by 2 orders of magnitude as compared to a homogeneous medium. The perfect agreement between measured and calculated single molecule image patterns implies that the method is suitable for routine orientation determination of single molecules at interfaces and in complex environments.

Figure 1 shows the setup used in the present study. Linearly polarized light from an Ar^+ laser with a wavelength of 514 nm is coupled into a single mode fiber. The light is collimated by a lens (L1) and reflected via a dichroic mirror onto the 6.3-mm-diam entrance aperture of an immersion oil microscope objective. A circular on-axis beam stop with a diameter of 3 mm removes the central part from the beam before being reflected at the dichroic mirror and entering the microscope objective. The resulting annular beam is focused to a diffraction-limited spot onto the thin sample on top of a cover glass. Opening angles between 38° and 58° contribute to the field distribution in the focus. The full angular range of fluorescence, collected by the same objective, passes the dichroic mirror and a holographic notch filter and is finally focused via a lens (L2) onto the 200-μm-diam active area of a single photon counting avalanche photodiode serving as confocal pinhole. The size of the back-projected image of the active area into the focal plane is about 1 μm in diameter. Single-molecule fluorescence images were recorded at excitation intensities far from saturation by raster scanning the sample through the focus (typically 256 $\times$ 256 pixels, 2 ms/pixel) using a linearized x-y-z piezo scan table and recording the number of counts for each pixel in a computer. The sample is a smooth, 20 nm thick

 0031-9007/00/85(21)/4482(4)$15.00

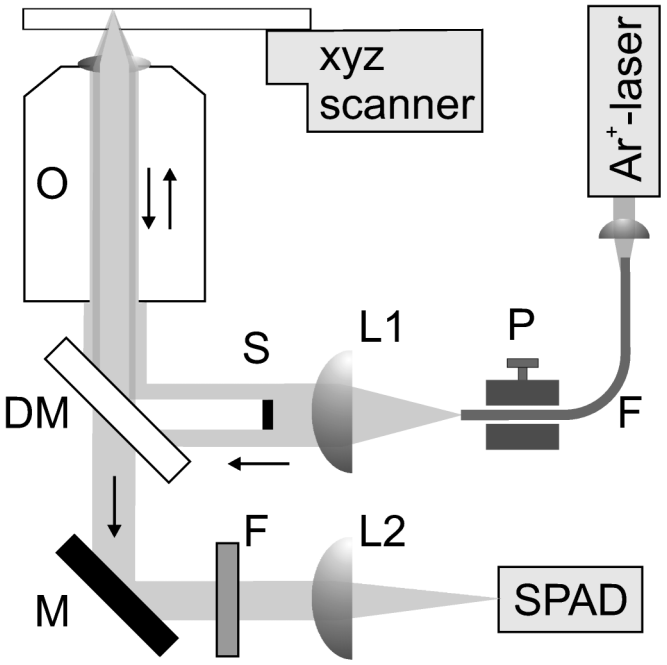

FIG. 1. Setup for annular illumination scanning confocal optical microscopy. L1: collimation lens ($f = 50$ mm); O: microscope objective (Leica, PL Fluotar, ×100, 1.3 numerical aperture, ∞); DM: dichroic mirror; M: mirror; F: holographic notch filter; L2: focusing lens ($f = 300$ mm); SPAD: single photon counting avalanche photodiode (EG&G SPCM 200); S: obstruction disk (3 mm diam); P: polarization controller (Polarite, L.O.T.); F single mode fiber.

polymethylmethacrylate (PMMA) film on a glass cover slip doped with 10^{-9} M of the dye *1,1'-dioctadecyl-3,3,3',3'-tetramethylindocarbocyanine* (DiI). The difference in the refractive indices of PMMA and glass is negligible. Standard fluorescence scanning confocal optical microscopy without annular illumination showed typical circular diffraction-limited single-molecule fluorescence spots with a full width at half maximum of 250 nm.

Figure 2 shows a typical single-molecule fluorescence image of the dye doped polymer film obtained with annular illumination and linear polarization as indicated by the arrow. Various spot shapes are observed ranging from bright spots with two less intense side lobes on both sides, oriented perpendicular to the direction of polarization (see, e.g., x) to less intense patterns consisting of four lobes of equal intensity situated in four corners of a square with one of its sides parallel to the excitation polarization (y). There are also double-lobed patterns (z), which exhibit two equally intense lobes oriented along the direction of polarization. Furthermore, various other patterns are observed that seem to represent squared superpositions of the three basic shapes. Each pattern is assigned to the fluorescence of a single molecule because (i) some patterns are truncated at the top side because of digital photobleaching during line-by-line image acquisition, (ii) some patterns exhibit intermittent dark spots due to excursions to

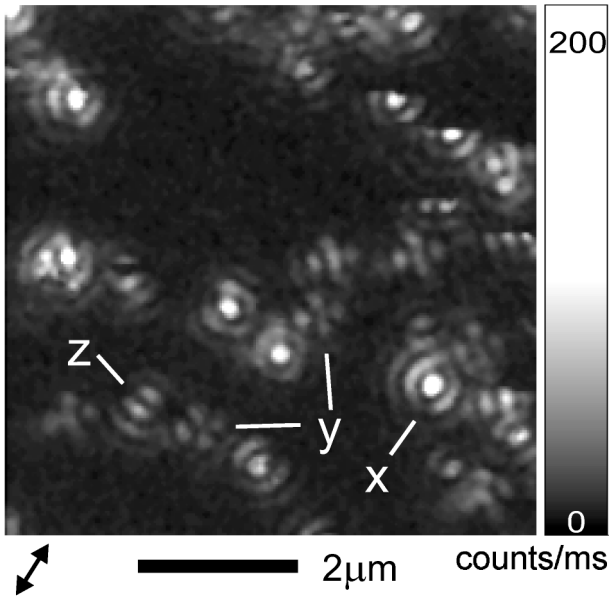

FIG. 2. Typical confocal single-molecule fluorescence image of DiI in a thin film of PMMA obtained with linearly polarized (arrow), annular illumination. The labeled patterns result from molecules that map the squared x, y, and z components of the electric field in the focus, respectively.

the triplet state, and (iii) the patterns are in perfect agreement with the assumption of a single, pointlike dipole mapping the field in the focus as to be discussed in the following.

We have calculated the distributions of the squared electric field components $\vec{\mathbf{E}}(\vec{\mathbf{r}})$ in the vicinity of the geometrical focus for four different geometries. Calculations for a homogeneous medium (i) with and (ii) without annular illumination have been performed using analytical results [19]. The multiple multipole method [20] was used to determine the electromagnetic field distribution in the presence of an interface that coincides with the focal plane (iii) with and (iv) without annular illumination. In this approach the scattered fields at the interface are expanded as an analytic series expansion of multipoles distributed along the interface. The coefficients in the expansion are determined numerically by requiring the boundary conditions in discrete points on the interface. Figure 3 shows the resulting field distribution ($|\vec{\mathbf{E}}|^2$) in the polarization plane (x, z) using annular illumination. Total internal reflection of the incident supercritical components leads to a standing wave pattern inside the higher optical density half space. At 5 nm beneath the interface, annular illumination reduces the spot size (FWHM of $|\vec{\mathbf{E}}|^2$) from ≈250 nm to ≈245 nm in the polarization plane (x, z) and from ≈185 nm to ≈150 nm in the (y, z) plane. However, this reduction is at the expense of more pronounced sidelobes. At 5 nm above the interface, the center spot splits up into two spots aligned along the direction of polarization and separated by ≈200 nm. This is because the double-lobed longitudinal field now dominates the

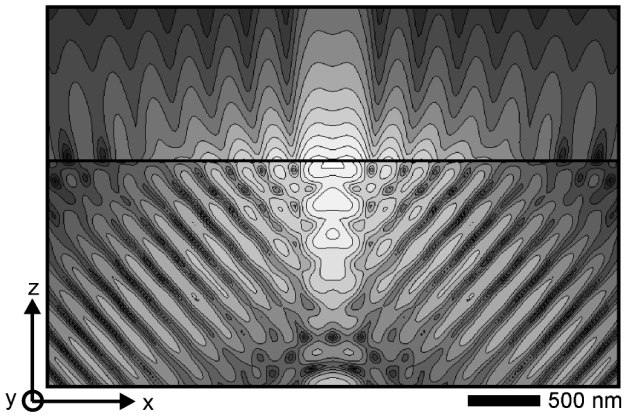

FIG. 3. Calculated field distribution ($|E|^2$, factor of 2 between adjacent contour lines) in the polarization plane (x, z) for linearly polarized, annular illumination in the presence of the interface. Angular range: 38°–58°, $\lambda = 514$ nm. Upper half space: air; lower half space: glass/polymer. The geometrical focal plane coincides with the polymer/air interface.

intensity distribution because of the boundary condition for normal field components at the interface.

It is interesting to note that the basic shapes of the distributions of the squared field components are nearly unaffected by the presence of the interface as compared to the homogeneous medium. However, their relative strength is strongly changed. We characterize the relative strength by the ratio of the maximum values found in the respective fluorescence pattern to the maximum fluorescence in the pattern where the dipole is parallel to the excitation polarization (here: x direction).

In Table I we collect the calculated relative magnitudes of the maximal E_y^2 and E_z^2 in a plane 5 nm below the focal plane obtained for the four investigated experimental configurations. We conclude that the four-lobed y patterns are observable only for annular illumination with an interface nearby. Indeed, the y patterns in Fig. 2 disappear when covering the sample by a thick layer of additional PMMA. To predict the visibility of the z patterns, the ratios of the collection efficiencies for a horizontal with respect to a vertical dipole are given in Table I in brackets [21]. It is found that in the presence of the interface, owing to total internal reflection, the collection efficiency for the vertical dipole is even slightly larger than for the horizontal dipole. We conclude that the z patterns are observable in all four configurations.

TABLE I. Calculated relative strength of the maximal E_x^2, E_y^2, and E_z^2 in a plane 5 nm below the polymer/air interface for different geometries. In brackets: ratios of the collection efficiencies for a horizontal with respect to a vertical dipole [21].

Illumination interface	Annular no	Full no	Annular yes	Full yes
$\max[E_x^2]/\max[E_y^2]$	108	315	11	33
$\max[E_x^2]/\max[E_z^2]$	3.8 (2)	8.1 (2)	4.5 (0.93)	10.5 (0.93)

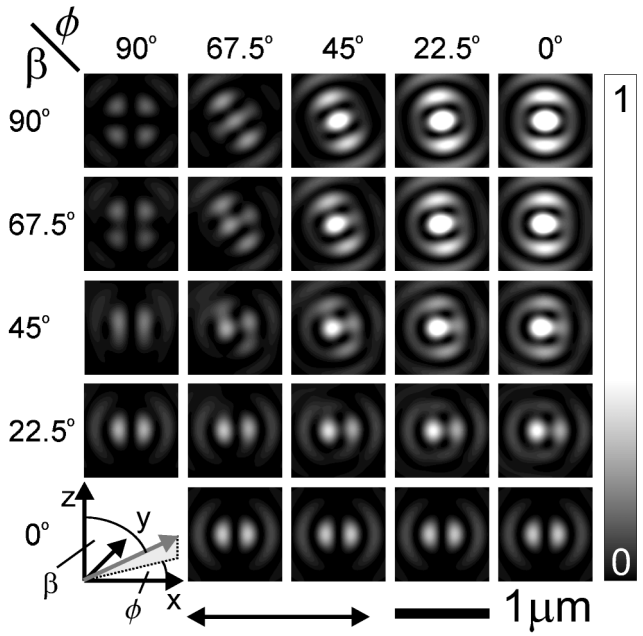

FIG. 4. Single-molecule fluorescence patterns 5 nm below the interface calculated from the field distribution according to (1). Coordinate system: definition of the dipole orientation angles β and ϕ with respect to the excitation polarization (double arrow).

The appearance of the enhanced longitudinal fields in the focus for annular illumination can be understood qualitatively by considering a geometrical optics picture.

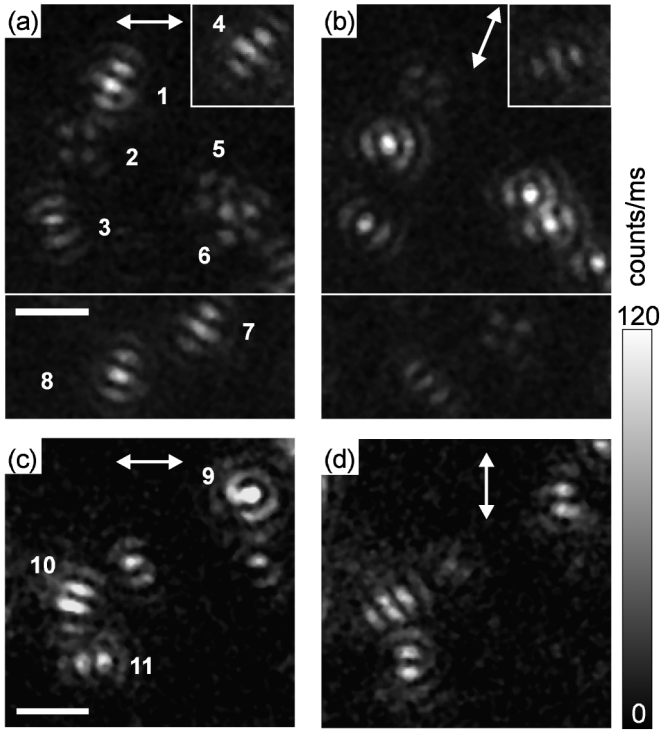

FIG. 5. Fluorescence patterns of molecules (a), (c) before and (b), (d) after polarization turned by ≃90°. The observed changes in the patterns are in agreement with a fixed dipole. Scale bar: 1 μm. Double arrows: excitation polarizations.

TABLE II. Orientation of the absorption dipole moment of single molecules, marked by numbers in Fig. 5, with respect to the polarization direction. Definition of ϕ and β as in Fig. 4.

Molecule	1	2	3	4	5	6	7	8	9	10	11
ϕ[°]	−45	90	45	−67.5	±90	90	−67.5	−30	45	−22.5	···
β[°]	67.5	67.5	90	90	90	67.5	90	90	−45	90	0

Decomposing the focused field into beams propagating at different angles with respect to the optical axis shows that by removing beams with large on-axis components of the propagation direction, the longitudinal field components in the focus will be enhanced as compared to the transverse components. On the other hand, the enhanced y patterns originate from the local polarization of the interface due to the longitudinal fields. This polarization generates a scattered field which interferes with the original beam and thus renders the observed y pattern. Hence, strong longitudinal fields are a prerequisite for generating strong y patterns close to interfaces.

For excitation intensities far from saturation the fluorescence rate $R(\vec{\mathbf{r}})$ of a single molecule located at $\vec{\mathbf{r}}$ is given by [22]

$$R(\vec{\mathbf{r}}) = c|\hat{\mathbf{d}} \cdot \vec{\mathbf{E}}(\vec{\mathbf{r}})|^2, \quad (1)$$

where $\hat{\mathbf{d}}$ is the unit vector along the absorption dipole moment of the molecule, $\vec{\mathbf{E}}(\vec{\mathbf{r}})$ is the electric field vector at the position of the molecule, and c is a constant.

Figure 4 shows annular illumination fluorescence patterns calculated according to Eq. (1) for differently oriented single molecules 5 nm below the polymer/air interface. The direction of the excitation polarization is indicated by the double arrow. The dipole orientation is defined by two angles, $-90° \le \phi \le 90°$ and $-90 \le \beta \le 90°$. Patterns for negative ϕ and β are not displayed since they can be obtained by symmetry considerations. The contrast settings indicated on the right of the matrix are the same for each pattern. Many of the calculated patterns are readily seen to reproduce measured shapes in Fig. 2. In particular, the patterns labeled by x, y, and z correspond to molecules oriented at $(\phi, \beta) = (0°, 90°)$, $(\phi, \beta) = (90°, 90°)$, and $\beta = 0°$, respectively.

In Figs. 5(a) and 5(c) the orientation of eleven molecules has been determined by comparison of the observed to calculated patterns in Fig. 4. The results are collected in Table II. Figures 5(b) and 5(d) show the same molecules after rotating the polarization by ≈90°. For all molecules, taking into account the changed distribution of field components, the new patterns can be explained by the same dipole orientation. This indicates that the molecules showed no significant orientational diffusion during the experiment (≈15 min).

Within the present method the orientation of a single molecule can be determined from a single image. By imaging the same molecules twice with orthogonal polarization, the method can be extended to determine the full orientation of single molecules far from an interface. Thus, the optical sectioning capabilities of confocal microscopy can be exploited. By using a higher numerical aperture of 1.4 and a larger central obstruction in the excitation beam the field distribution in the focus can be further improved. The demonstrated method is well suited for monitoring rotational diffusion of single molecules in complex environments.

The authors acknowledge stimulating discussions with M. Prummer, J.-M. Segura, and W. Trabesinger, continuous interest and support by Professor U. P. Wild, as well as mechanical support by A. Hunkeler and B. Lambillotte. This work was supported by ETH-Zürich and the University of Rochester.

*Electronic address: hecht@phys.chem.ethz.ch

[1] *Single-Molecule Optical Detection, Imaging and Spectroscopy,* edited by T. Basché, W. E. Moerner, M. Orrit, and U. P. Wild (VCH, Weinheim, 1997).
[2] X. S. Xie and J. K. Trautman, Annu. Rev. Phys. Chem. **49**, 441480 (1998).
[3] E. Betzig and R. J. Chichester, Science **262**, 1422 (1993).
[4] J. J. Macklin *et al.,* Science **272**, 255 (1996).
[5] J. A. Veerman *et al.,* J. Microsc. **194**, 477 (1999).
[6] S. Weiss, Science **283**, 1676 (1999).
[7] T. Ha *et al.,* Phys. Rev. Lett. **77**, 3979 (1996).
[8] H. P. Lu, L. Xun, and X. S. Xie, Science **282**, 1877 (1998).
[9] D. A. Vanden Bout *et al.,* Science **277**, 1074 (1997).
[10] L. Fleury *et al.,* Phys. Rev. Lett. **84**, 1148 (2000).
[11] T. Ha *et al.,* J. Phys. Chem. B **103**, 6839 (1999).
[12] T. Ha *et al.,* Phys. Rev. Lett. **80**, 2093 (1998).
[13] T. Plakhotnik *et al.,* Opt. Commun. **114**, 83 (1995).
[14] T. Ha *et al.,* Proc. Natl. Acad. Sci. U.S.A. **93**, 6264 (1996).
[15] S. A. Empedocles, R. Neuhauser, and M. G. Bawendi, Nature (London) **399**, 126 (1999).
[16] F. Güttler *et al.,* Chem. Phys. **211**, 421 (1996).
[17] J. Sepiol *et al.,* Chem. Phys. Lett. **273**, 444 (1997).
[18] R. M. Dickson, D. J. Norris, and W. E. Moerner, Phys. Rev. Lett. **81**, 5322 (1998); A. P. Bartko and R. M. Dickson, J. Phys. Chem. B **103**, 3053 (1999); **103**, 11 237 (1999).
[19] B. Richards and E. Wolf, Proc. R. Soc. London A **253**, 358 (1959); R. Kant, J. Mod. Opt. **40**, 337 (1993).
[20] Ch. Hafner, *The Generalized Multiple Multipole Technique for Computational Electrodynamics* (Artech, Boston, MA, 1990).
[21] The values for a homogeneous medium were calculated according to [13]. The values for the interface were determined numerically.
[22] T. Plakhotnik, E. Donley, and U. P. Wild, Annu. Rev. Phys. Chem. **48**, 181 (1997).